Available online at www.sciencedirect.com

jmr&t Journal of Materials Research and Technology

journal homepage: www.elsevier.com/locate/jmrt

Original Article

Analysis of the protection performance of admixed citronella and myrrh essential oil extracts on high carbon steel corrosion in CH_3COOH and $C_6H_8O_7$ solution

Roland Tolulope Loto[*]

Department of Mechanical Engineering, Covenant University, Ota, Ogun State, Nigeria

ARTICLE INFO

Article history:
Received 2 October 2022
Accepted 7 November 2022
Available online 12 November 2022

Keywords:
Corrosion management
Inhibitor
Steel
Plant extract

ABSTRACT

Protection performance of admixed citronella and myrrh essential oil extract (CNM) on the corrosion resistance of high carbon steel (HCS) in 3 M of CH_3COOH and $C_6H_8O_7$ solution was evaluated by potentiodynamic polarization, open circuit potential measurement, weight loss measurement, x-ray diffractometry and ATF-FTIR spectroscopy. Results showed CNM performed effectively in CH_3COOH with optimal inhibition of 87.47% and 80.12% at 1.67% concentration from potentiodynamic polarization and weight loss. CNM performed poorly in $C_6H_8O_7$ solution with highest value of 41.29% and 43.81% at 1.67% CNM concentration from both tests. In both acids inhibition efficiency increased with increase in CNM concentration coupled with the exhibition of mixed-type inhibition effect. Open circuit potential plots show CNM significantly reduces the activation barrier for HCS to corrode wherewith the plots in the presence of CNM extract where significantly electropositive compared to the plot from $C_6H_8O_7$ solution without CNM. In CH_3COOH, the action of protonated CNM molecules and $CH_3CO_2^-$ anions results in the formation of complexes that increases the reactivity of HCS surface and its thermodynamic tendency to corrode despite effective inhibition performance. X-ray diffractometry shows admixed extract caused significant decrease in intensity/counts for diffraction peaks of Fe_2O_3 and Fe_3O_4 compounds on the spectrum plots compared to the plots without the extracts. ATF-FTIR spectroscopy shows significant reduction in transmittance at specific range of wavenumbers occurred within CNM/CH_3COOH solution after corrosion, and on HCS surface after corrosion in the presence of the extracts compared to CNM/CH_3COOH before corrosion. This contrast the results obtained from CNM/$C_6H_8O_7$ solution.

* Corresponding author.
E-mail address: tolu.loto@gmail.com.

https://doi.org/10.1016/j.jmrt.2022.11.048

1. Introduction

Ferrous alloys represent the fourth most applied metallic alloy globally. Their economic relevance worldwide stems from often being a relevant indicator of a nation's industrial output [1]. The use of ferrous alloys is prevalent in the construction industry, marine industry, vehicular industry, aerospace industry, energy generating industry, mining industry etc. It represents about half of the total tonnage of motor cars. Carbon steels are ferrous alloys comprising about 85% of the total steels produced. They have almost universal application in most industries due to their availability, ease of construction, cost, physical properties, metallurgical properties and mechanical properties. The vulnerability of carbon steels to corrosion when exposed to environments (e.g. industrial) laden with corrosive anions is a major setback to their productive utilization due to lack of passivating elements [2]. Industrial processes such as acid descaling, movement of acid, pickling of ores, boiler applications, heat transfer reactions of heavy water reactor etc. Poses major problem to the operational lifespan of carbon steels leading to frequent replacements of the steels. Corrosion is an inherent chemical/electrochemical process that occurs naturally on metallic alloys at high energy states, returning them to their natural state in the form of ores, compounds etc. It is a process resulting from the interaction of metallic alloys with their environments. The consequential effect of corrosion is encapsulated in the form of high cost of maintenance, frequent damages to metallic components and equipment's, manufacturing losses, and costly industrial timeouts [3–5].

$C_6H_8O_7$ is a weak organic acid which forms naturally in citrus fruits and is estimated to have a worldwide production of about 1.4 million tons in 2004 [6]. The acid is utilized as an intermediate chemical in the production of cosmetics, seasonings, disinfectants, beverages, and also in a wide range of industrial processes (oil well acidizing, picking, chelating compound) [7–11]. The occurrence of $C_6H_8O_7$ within these products/processes corrodes carbon steel parts of components, machineries and structures resulting in very high possibility of product/process contamination with corrosion byproducts. CH_3COOH is a byproduct of fermentation, oxidation of ethanol and carbonylation of methanol. It is the 33rd most manufacture reagent in the United States with a global demand of about 6.5 million metric tons per year [12]. It is utilized in the production of acetic anhydride, acetic esters, chloracetic acid, vitamins, insecticides, dyes, acid descaling etc. [13]. Corrosion of carbon steels in CH_3COOH is prevalent in industrial processes associated with chemical and petrochemical industries [14]. Most research on carbon steels in CH_3COOH acids have focused on the influence of CH_3COOH acid on CO_2 corrosion of carbon steels while a few others focused on corrosion in CH_3COOH. Aria et al., studied the mechanism and kinetics of carbon steel corrosion in deaerated aqueous CH_3COOH solutions. Results show CH_3COOH influenced the corrosion reaction process [15]. Anusuya and Prasanna studied the effect of CH_3COOH corrosion on carbon steel in CO_2–H_2S solution at above room temperature Results show the effect is more prevalent at higher pressure of H_2S resulting in pitting corrosion [16]. George and Nesic, investigated the corrosion behavior of mild steel in the presence of CH_3COOH and CO_2 Results show that CH_3COOH affects predominantly the cathodic corrosion reaction at elevated temperatures [17]. Okafor and Nesic investigated the effect of CH_3COOH on the corrosion behavior of X65 and C1018 carbon steel in vapor-H_2O two-phase stratified flow CO_2. Corrosion rates were observed to increase with increase in CH_3COOH concentration as result of H_2 ions by CH_3COOH to the cathodic reaction [18]. Singh and Mukherjee studied the kinetics of mild steel corrosion in aqueous CH_3COOH acid solution. Corrosion rate was observed to increase to a certain optimum before decreasing [19].

Methods and techniques of carbon steel corrosion inhibition have varied significantly in the past 2 decades due to increased knowledge of corrosion reaction processes and the economic effect of corrosion damage [20]. The most versatile method of corrosion prevention in corrosive environments is the application of corrosion inhibitors [21]. These compounds stifle the electrochemical mechanisms associated with corrosion of carbon steels. The mechanism by which inhibitors act are; a) chemical adsorption of metallic surfaces, b) evolution of protective oxide and c) formation of protective precipitates on the metallic surface. While inorganic compounds such as chromates, borates, nitrites, silicates etc. and organic derivatives have been proven to be effective corrosion inhibitors, their continual use has been severely restricted due to government regulations and safety reasons. Extracts of plants are a rich source phytochemical compounds associated with corrosion inhibition [22–29]. Previous research on application of corrosion inhibitors on carbon steel in citric and acetic acid have given appreciable results [30–34]. Increase in the industrial production of citric and acetic acid results in increase in corrosion of carbon steels in such applications hence the need to protect the steels from corrosion. This article investigates the synergistic effect of citronella and myrrh oil on the corrosion inhibition of high carbon steel in citric and acetic acid solution.

2. Experimental methods

2.1. *Materials and preparation*

High carbon steel (HCS) test piece with radial dimension of 1.2 cm diameter was determined to have elemental composition of 0.91% C, 0.54% Mn, 0.03% S, 0.06% P and 98.4% Fe from energy dispersive X-ray microanalysis with PhenomWorld scanning electron microscope. The HCS test piece was split into individual smaller test pieces with hand cutting tool into specific dimensions of 1 cm (length x breadth) for weight loss measurement. HCS test pieces prepared for electrochemical analysis and open circuit potential measurement were fixed to a Cu strand with soldering lead before implanting in prehardened resin admixture. The observable surface of the steel was grinded with emery papers (60, 300, 600, 1000 and 1500 grits) and polished with 6 μm diamond solution before washing with distilled H_2O and acetone. Citonella and myrrh (CNM) essential oil extracts purchased from NOW Foods, USA were added together in equal ratios and prepared in

volumetric concentrates of 0%, 0.42%, 0.82%, 1.25% and 1.67% respectively in 300 mL each of 3 M CH_3COOH and $C_6H_8O_7$ solutions.

2.2. Potentiodynamic polarization and open circuit potential measurement

Corrosion measurement test (potentiodynamic polarization and open circuit potential measurement) was carried out at 308 K (room temperature) using a Digi-Ivy 2311 potentiostat. The potentiostat connected to a computer, consist of threefold electrode configuration located within a translucent beaker holding the acid-extract solution. The electrodes are HCS test piece electrode with observable surface area of 1.13 cm^3, Ag/AgCl standard electrode and Pt strand auxiliary electrode. Polarization curves were plotted at sweep rate of 0.0015 V/s from −1.5 V and +1.5 V. Corrosion current density C_{cd} (A/cm^2) and corrosion potential, C_{pt} (V) values were obtained by Tafel derivation. Corrosion rate, C_{rt} (mm/y) was computed from the numerical expression below;

$$C_{RT} = \frac{0.00327 \times C_j \times E_q}{D} \quad (1)$$

where Eq is the equivalent weight (g) of HCS, 0.00327 is the corrosion constant and D represent density (g/cm^3). Inhibition efficiency, I_{ef} (%) was determined from the relationship below;

$$I_{ef} = \left[1 - \left(\frac{C_{rt2}}{C_{rt1}}\right)\right] \times 100 \quad (2)$$

C_{rt1} and C_{rt2} are HCS corrosion rates without and with the extracts. Polarization resistance, P_{rt} (Ω) was determined from below;

$$P_{rt} = 2.303 \frac{B_a B_c}{B_a + B_c}\left(\frac{1}{I_{cr}}\right) \quad (3)$$

Ba and Bc represents the anodic and cathodic Tafel slopes (V/dec).

2.3. ATF-FTIR spectroscopy and optical microscopy characterization

0.42% CNM concentration/3 M CH_3COOH and $C_6H_8O_7$ solution, preceding and after corrosion test were analyzed under infrared particle emissions with Bruker Alpha FTIR (Fourier transform infrared spectroscopy) spectrometer limited to wavelength span of 375 and 7500 cm-1, and accuracy of 0.9 cm−1. Spectral patterns were observed and interpreted with the conventional ATF-FTIR (Attenuated total reflectance-Fourier transform infrared spectroscopy) table. The reactive groups which influenced the redox reaction processes were illustrated in table format. Optical representations of HCS test pieces preceding and after corrosion test with and without the presence of the CNM was performed with Mustech digital microscope.

2.4. Weight loss measurement

Weight of HCS test pieces were calculated after suspension in 300 mL of the acids-extract solution for 168 h. HCS weight determination was gotten at 24 h interval. Corrosion rate, Crt (mm/y) was obtained from the relationship below;

$$C_{rt} = \left[\frac{87.6 W_L}{DAt}\right] \quad (4)$$

WL represents weight loss (g), D indicates the density (g/cm3) of HCS, t represents time (h), A is the total exterior area of the HCS specimen (cm2) and 87.6 indicates corrosion rate constant. Inhibition efficiency (Ief) was determined from the following relationship;

$$I_{ef} = \left[\frac{W_{L2} - W_{L2}}{W_{L1}}\right] \times 100 \quad (5)$$

WL1 represents weight loss without extract concentrations and WL2 with extract concentration.

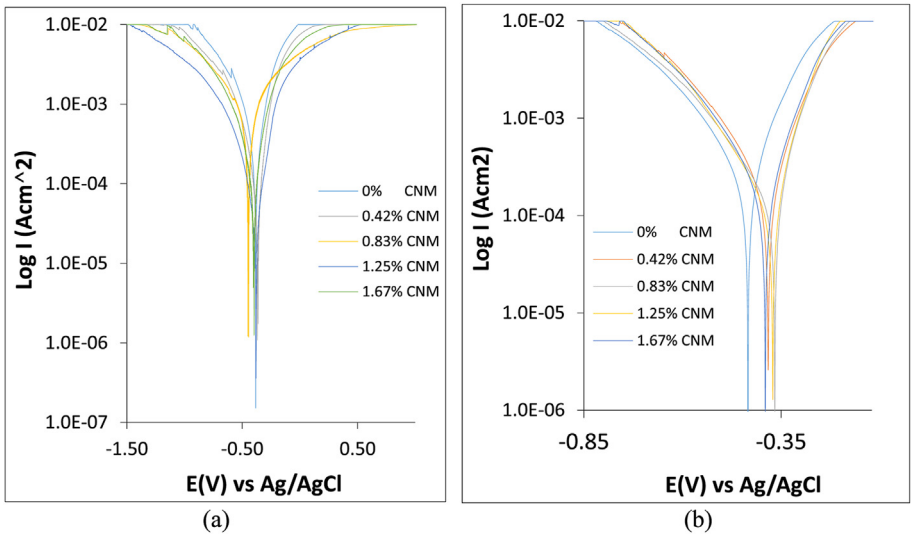

Fig. 1 − Potentiodynamic polarization plots of HCS corrosion at 0%−1.67% CNM extract concentrations in (a) CH_3COOH acid and (b) $C_6H_8O_7$ acid.

2.5. X-ray diffractometry

X-ray diffraction plots and pattern list of the phase compounds, precipitates and metallic complexes on HCS (samples A, B and E) surface in the presence of and without the oil concentrates were produced after analysis with Rigaku D/Max-lllC X-ray diffractometer at scanning rate of 20/min in the 2 to 500 at room temperature with a CuKa radiation set at 40 kV and 20 mA in 2θ. The diffraction data (relative intensity) obtained was matched with the standard data of minerals from the mineral powder diffraction file (ICDD) which contained and includes the standard data of more than 3000 minerals.

3. Result and discussion

3.1. Potentiodynamic polarization studies

Cathodic-anodic polarization plots for HCS corrosion in 3 M CH3COOH and C6H8O7 acid at 0%, 0.42%, 0.83%, 1.25% and 1.67% CNM extract concentration are shown in Fig. 1(a) and (b). Fig. 2(a) and (b) is a close-up view of the corrosion potential variations of the polarization plots. Table 1 shows the polarization data obtained from the electrochemical test in both acids. Comparison of the corrosion rate results of HCS at 0% CNM concentration in both acids shows $C_6H_8O_7$ acid is slightly more corrosive than CH_3COOH acid with comparative values of 1.55 mm/y to 1.26 mm/y. $C_6H_8O_7$ being a weak organic tripotic acid gives off $3H_3O+$ and $C_6H_5O_7^{3-}$ ion in H_2O with respect to the equations below;

$$C_6H_8O_7\ (aq) + H_2O(l) \rightleftharpoons C_6H_7O_7^-(aq) + H_3O+\ (aq) \quad (6)$$

$$C_6H7O_7^-(aq) + H_2O(l) \rightleftharpoons C_6H_6O_7^{2-}(aq) + H_3O+\ (aq) \quad (7)$$

$$C_6H_6O_7^{2-}(aq) + H_2O(l) \rightleftharpoons C_6H_5O_7^{3-}(aq) + H_3O+\ (aq) \quad (8)$$

$C_6H_5O_{7\ (aq)}^{3-}$ is a tricarboxylic acid trianion resulting from the deprotonation of the 3 carboxy active groups of $C_6H_8O_7$ acid. CH_3COOH being a monoprotic weak organic acid reacts with H_2O to produce CH_3CHOO^- ions and H_3O^+ ions, according to the following equation;

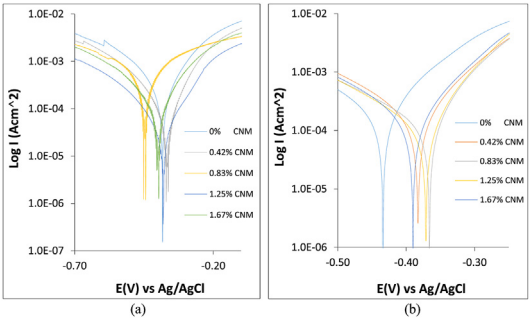

Fig. 2 – Close-up view of the corrosion potential variations of the polarization plots at 0%–1.67% CNM extract concentrations in (a) CH_3COOH acid and (b) $C_6H_8O_7$ acid.

$$CH_3COOH + H_2O \rightleftarrows CH_3CO_2^- + H_3O^+$$

$CH_3CO_2^-$ is a monocarboxylic acid anion produced from the removal of 1 proton from the carboxy active group of CH_3COOH acid. The higher ionization potential and acidity of $C_6H_8O_7$ compared to CH_3COOH results in relatively higher rate of corrosion of HCS as shown in the corrosion rate results. Both acids react with the substrate metal (Fe) of HCS resulting in their release into the acid solution as corrosion products.

$C_6H_8O_7$ and CH_3COOH reacts with HCS according to equations (9) and (10)

$$Fe + C_6H_8O_7 \rightarrow FeC_6H_6O_7 + H_2 \quad (9)$$

$$Fe + 2CH_3CO_2H \rightarrow Fe(CH_3CO_2)_2 + H_2 \quad (10)$$

The release of H^+ results in the loss of electrons from HCS when it transforms into its ionic form. Addition of CNM extract at various concentrations changed the dynamics of the corrosion reaction process. At 0.42% CNM concentration, corrosion rate of HCS decrease to 0.44 mm/y in CH_3COOH and 1.31 mm/y in $C_6H_8O_7$. These values correspond to corrosion current density of 3.85×10^{-5} A/cm^2 and 1.15×10^{-4} A/cm^2. The corresponding inhibition efficiency values at 0.83% CNM concentration are 65.16% in CH_3COOH and 15.55% in $C_6H_8O_7$ acid. This shows CNM performs effectively in CH_3COOH compared to $C_6H_8O_7$ acid were its performance is poor. These corresponding values indicate protonated molecules of CNM extract are unable to suppress the oxidation reactions on HCS responsible for $FeC_6H_6O_7$ formation in $C_6H_8O_7$. As a result, more corrosion products are released into $C_6H_8O_7$ solution. In CH_3COOH solution, CNM molecules effectively prevented the formation of $Fe(CH_3CO_2)_2$ corrosion products into the aqueous media. Further increase in CNM concentration results in progressive decrease in corrosion rate values of HCS and increase in inhibition efficiency of CNM. Corrosion rate of HCS decreased to 0.16 mm/y at 1.67% CNM concentration in CH_3COOH compared to 0.91 mm/y in $C_6H_8O_7$. These values correspond to 87.47% and 41.29%. However, the effective performance of CNM in CH_3COOH is overshadowed by its poor performance in $C_6H_8O_7$.

Observation of the corrosion potential values shows anodic-cathodic shift of the potentials with respect to CNM concentration in CH_3COOH acids. The optimal anodic shift occurred at 0.83% CNM concentration (−0.451 V). Cathodic shift occurred at 0.42% and 1.25% CNM concentration. However, variation in corrosion potential at all concentrations signifies mixed inhibition effect of CNM extract in CH_3COOH acid. In $C_6H_8O_7$ acid, cathodic potential shift occurred at 0.83% CNM concentration while at other concentrations anodic potential shift dominated. This observation aligns with the weak inhibition effect of CNM extract in $C_6H_8O_7$ acid where protonated molecules of CNM were unable to limit the oxidation of HCS.

3.2. Weight loss measurement and optical microscopy analysis

Data plots for weight loss measurement of HCS in 3 M CH_3COOH and $C_6H_8O_7$ acid solutions at 0%, 0.42%, 0.83%, 1.25%

Table 1 – Potentiodynamic polarization data for HCS corrosion in CH_3COOH and $C_6H_8O_7$ solution at 0%–1.67% CNM.

Sample	CNM Conc. (%)	HCS C_R (mm/y)	CS ξ_F (%)	C_I (A)	C_J (A/cm^2)	C_P (V)	R_p (Ω)	B_c (V/dec)	B_a (V/dec)
CH_3COOH Solution									
A	0	1.26	0	1.83E-04	1.11E-04	−0.383	140.30	−7.259	8.96
B	0.42	0.44	65.16	6.36E-05	3.85E-05	−0.370	404.10	−8.203	11.690
C	0.83	0.39	69.26	5.61E-05	3.40E-05	−0.451	508.45	−4.874	6.763
D	1.25	0.26	79.21	3.80E-05	2.30E-05	−0.381	677.00	−7.717	8.553
E	1.67	0.16	87.47	2.29E-05	1.39E-05	−0.397	876.70	−7.370	8.545
$C_6H_8O_7$ Solution									
A	0	1.55	0	2.25E-04	1.36E-04	−0.381	114.20	−6.942	9.430
B	0.42	1.31	15.55	1.90E-04	1.15E-04	−0.383	135.50	−7.024	10.610
C	0.83	1.18	24.14	1.70E-04	1.03E-04	−0.366	150.90	−6.378	11.530
D	1.25	1.05	32.29	1.52E-04	9.21E-05	−0.371	169.00	−6.931	12.340
E	1.67	0.91	41.29	1.32E-04	7.99E-05	−0.390	186.10	−7.160	11.070

and 1.67% CNM concentration are shown from Figs. 3(a) to 4(b). Fig. 3(a) and (b) shows the plots of HCS corrosion rate versus exposure time from CH_3COOH and $C_6H_8O_7$ solution while Fig. 4(a) and (b) shows the corresponding plots of CNM inhibition efficiency versus exposure time from both acid solutions. Table 2 shows the data obtained at 168 h of exposure in both acids. Fig. 5(a)–(e) shows the optical images of HCS before corrosion test, after corrosion without CNM extract in CH_3COOH and $C_6H_8O_7$ acid solution, and after corrosion in CH_3COOH and $C_6H_8O_7$ acid solution at 1.67% CNM extract concentration. Observation of the data in Table 2 shows CNM extract performed more effectively in CH_3COOH compared to $C_6H_8O_7$ solution. At 168 h of exposure, the final corrosion rate values of HCS from CH_3COOH solution ranges from 2.638 mm/y at 0.42% CNM concentration to 0.525 mm/y at 1.67% CNM concentration. The optical images in Fig. 5(b) and (c) attests to the debilitating action of $CH_3CO_2^-$ and $C_6H_5O_7^{3-}$ anions on HCS surface where corrosion is clearly visible, although the extent of damage higher in Fig. 5(b). Comparing the inhibition efficiency values, CNM exhibited effective protection performance in CH_3COOH solution as proven in Fig. 5(d) where the oil extract protected the entire HCS surface and stifled the redox reaction processes. The inhibition values in CH_3COOH solution ranged from 53.06% at 0.42% CNM to 80.12% at 1.67% CNM concentration. This signifies concentration dependent performance of CNM extract in CH_3COOH solution.

Observation of the corrosion rate plot versus exposure time [Fig. 3(a) and (b)] shows significant decrease in corrosion rate values from initiation (24 h) to termination of HCS exposure (168 h) in both acids at all CNM concentrations with respect to exposure time. In Fig. 3(a) the extreme values ranged between 2.173 mm/y and 5.215 mm/y at 24 h of exposure before decreasing to values between 0.927 mm/y and 3.187 mm/y at 72 h of exposure where relative stability was attained. At 168 h of exposure the corrosion rate values culminated between 0.525 mm/y and 2.638 mm/y. The plot in Fig. 3(b) initiated at extreme values between 12.167 mm/y and 8.256 mm/y (24 h), and progressively decreased continually to values between 7.015 mm/y and 3.942 mm/y at 168 h. The plots in both figures [Fig. 3(a) and (b)] shows corrosion rates of HCS in both acid solutions is a direct proportional function of the amount of protonated extract solution in the acid media with increase in exposure time. Secondly, the rate of corrosion in $C_6H_8O_7$ is significantly higher than in CH_3COOH.

The plots in Fig. 4(a) shows significant and continual increase in inhibition efficiency at 1.67% CNM concentration. At

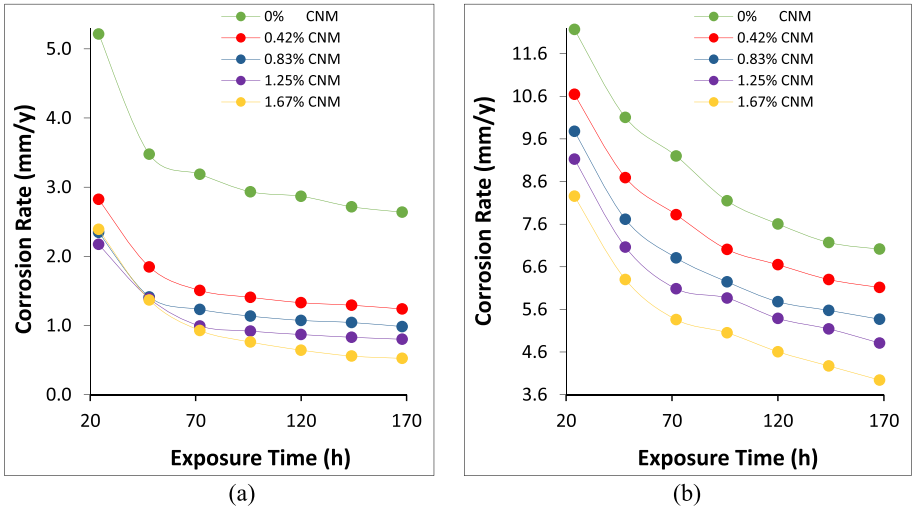

Fig. 3 – Plots of HCS corrosion rate versus exposure time in (a) CH_3COOH and (b) $C_6H_8O_7$ at 0%–1.67% CNM concentration.

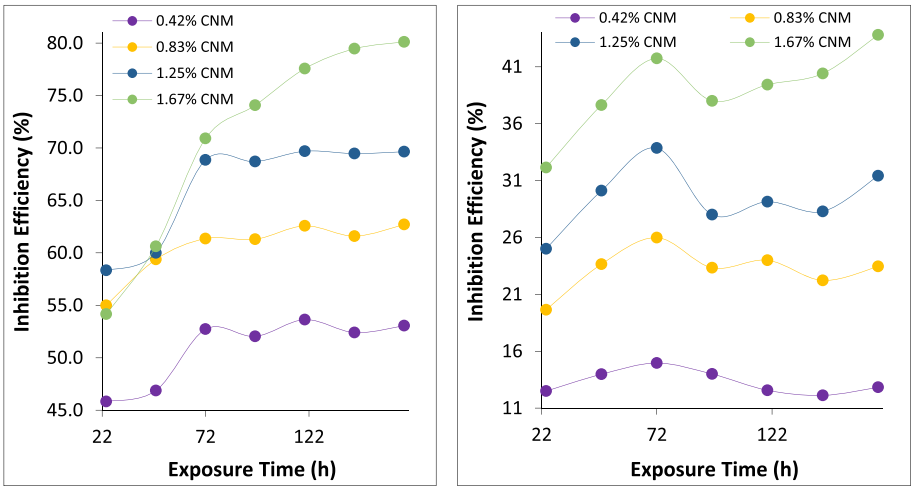

Fig. 4 – Plots of CNM inhibition efficiency versus exposure time in (a) CH_3COOH and (b) $C_6H_8O_7$ at 0.42%–1.67% CNM concentration.

0.42% and 1.25% CNM concentration, inhibition efficiency attained relative stability at 72 h of exposure with values of 68.86% and 52.72%. Beyond 72 h of exposure relative stability was attained till 168 h with a final inhibition value of 69.65% and 53.06%. Inhibition efficiency at 0.83% CNM concentration was relatively stable after 48 h of exposure. Comparing these observations to Fig. 4(b), inhibition efficiency values vary passively with exposure time. The plots initiated (24 h) at extreme inhibition values between 32.14% and 12.5% before culminating at 168 h with extreme values of 43.81% and 12.83%.

3.3. *Open circuit potential measurement*

Open circuit potential (OCP) plots of HCS corrosion in CH_3COOH and $C_6H_8O_7$ acid at specific CNM concentrations is shown in Fig. 6(a) and (b). The OCP plots in Fig. 6(a) significantly contrast the plots in Fig. 6(b). The plots in Fig. 6(a) shows OCP plot at 0% CNM concentration is significantly more electropositive than the plots at 0.42% and 1.67% CNM concentration. The plot initiated at −0.334 V (0s) before briefly shifting to electronegative value till 400s (−0.338 V). Before 1400s (−0.335 V), the plot exhibited active–passive transition behavior beyond which a progressive decrease in potential occurred till 11000s at −0.370 V. The decrease in potential is due to oxidation of HCS surface leading to corrosion of the substrate metal with respect to time. Addition of CNM extract at 0.42% and 1.67% concentration increased the thermodynamic tendency of HCS to corrode despite effective inhibition efficiency from potentiodynamic polarization studies. This observation is due to the formation of complexes on HCS surface between the corrosive anions from CH_3COOH and protonated CNM molecules. The plots at 0.42% and 1.67% CNM concentration initiated at −0.391 V and −0.422 V respectively. The plot at 0.42% CNM was relatively stable for 600s till −0.376 V before decreasing progressively to −0.386 V at 2200s. Beyond this point it was relatively stable culminating at −0.396 V (11000s). Whereas the plot 1.67% CNM concentration sharply decreased to −0.414 V at 201.4s before progressively increasing to relative electropositive values till 1000s at −0.396 V. Beyond this point on the plot visible active–passive transition behavior was observed on the plot till 11000s at −0.395 V.

Observation of the plot in Fig. 6(b) shows CNM significantly decreases the thermodynamic tendency of HCS to corrode in $C_6H_8O_7$ acid despite the poor inhibition performance of CNM in the acid. At 74s of exposure, the plot at 0% CNM concentration significantly shifted to electronegative values due to the redox reaction processes occurring on HCS surface in $C_6H_8O_7$ acid till −0.393 V at 1039.41s. Beyond this point, the plot was relatively stable till −0.385 V at 11000s. Comparing

Table 2 – Weight loss data obtained at 168 h of exposure in CH_3COOH and C_6H_8O7 acids.

CH_3COOH				C_6H8O_7			
CNM Extract Concentration (%)	Weight Loss (g)	Corrosion Rate (mm/y)	Inhibition Efficiency (%)	CNM Extract Concentration (%)	Weight Loss (g)	Corrosion Rate (mm/y)	Inhibition Efficiency (%)
0	0.085	2.638	–	0	0.226	7.015	–
0.42	0.040	1.238	53.059	0.42	0.197	6.115	12.832
0.83	0.032	0.984	62.706	0.83	0.173	5.370	23.451
1.25	0.026	0.801	69.647	1.25	0.155	4.811	31.416
1.67	0.017	0.525	80.118	1.67	0.127	3.942	43.805

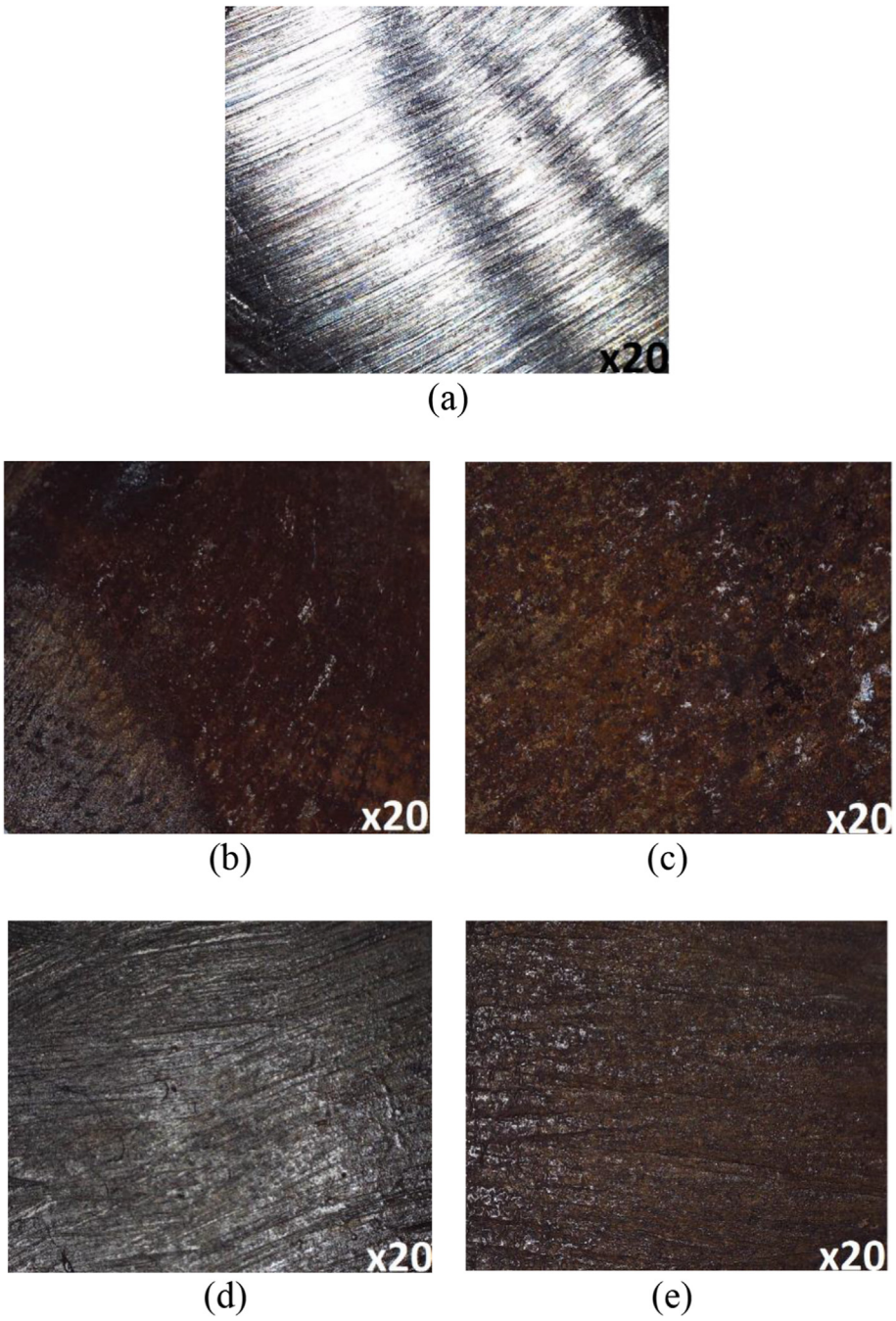

Fig. 5 – Optical images of HCS (a) before corrosion test, after corrosion without CNM extract in (b) CH_3COOH and (c) $C_6H_8O_7$ acid solution, and after corrosion in (d) CH_3COOH and (e) $C_6H_8O_7$ acid solution at 1.67% CNM extract concentration.

this to the plots at 0.42% and 1.67% CNM concentration; the plots at these concentrations exhibited similar plot configuration to the plot at 0% CNM concentration. They attained relative thermodynamic stability at 1600s and 3200s (−0.377 V and −0.375 V) before culminating at −0.375 V at 11000s. However, observation of the plots shows active–passive transition behavior which is much more visible on the plot at 0.42% CNM concentration. The difference in thermodynamic behavior on the OCP plots of HCS in $C_6H_8O_7$ compared to CH_3COOH is due to the mechanism of interaction and adsorption CNM molecules on HCS surface. However, the molecules are not sufficient to prevent the corrosion of HCS. The molecules reduce the thermodynamic tendency of HCS to corrosion while simultaneously unable to reduces the kinetic of the corrosion process at specific sites on HCS.

3.4. *X-ray diffractometry*

X-ray diffraction plots of HCS before corrosion test, after corrosion in CH_3COOH and $C_6H_8O_7$ solution without CNM

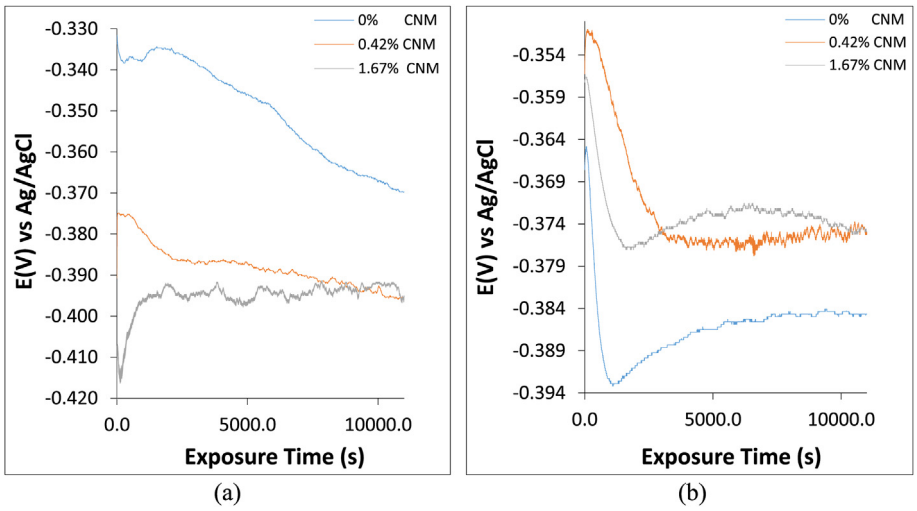

Fig. 6 – Open circuit potential plots of HCS corrosion at 0%, 0.42% and 1.67% CNM extract concentrations in (a) CH_3COOH acid and (b) $C_6H_8O_7$ acid.

extract, and after corrosion in the presence of CNM extract are depicted from Fig. 7(a) to 7(e). Fig. 7(a), 7(b) and 7(c) depict the diffraction plots for HCS before corrosion, after corrosion in CH_3COOH solution (0% CNM concentration) and after corrosion in $C_6H_8O_7$ solution (0% CNM concentration). Fig. 7(d) and (e) depict the diffraction plots for HCS after corrosion in CH_3COOH solution and $C_6H_8O_7$ solution at 1.67% CNM concentration. The diffraction plots provide information on the effect of CNM extract on the crystallographic properties and phase compounds of HCS. The diffraction plot in Fig. 7(a) shows high intensity/counts for Fe_2O_3, Fe_3O_4 and FeO(OH). Fe_2O_3 commonly identified as rust is produced from interaction between Fe in HCS with O_2 and H_2O in the environment. Fe_3O_4 identified as Iron (II, III) oxide occurred at lower intensity/counts compared to Fe_2O_3 while FeO(OH), a corrosion product was identified at lower intensity/counts compared to Fe_2O_3 and Fe_3O_4. These compounds appeared on the diffraction plots at intensity and counts of 520, 280, 150 and 300 corresponding to 2Θ angles of 10.4, 20.44, 30.84 and 48.86. The diffraction plots in Fig. 7(b) and (c) shows higher intensity/counts for Fe_2O_3 and Fe_3O_4 phase compounds compared to Fig. 7(a) due to corrosion of HCS in CH_3COOH and $C_6H_8O_7$ without CNM extract. In Fig. 7(b), the dominant intensity/counts occurred at 450, 550 and 550 (at 2Θ angle of 20.50, 30.86 and 53.46) while in Fig. 7(b) the dominant intensity counts occurred at 450 and 550 (at 2Θ angle 20.8 and 48.84). In the presence of CNM extract, significant decrease in intensity/counts for the diffraction peaks occurred in Fig. 7(d) and (e). In Fig. 7(d), the highest peaks (Fe_2O_3 and Fe_3O_4) occurred at intensity/counts of 170 and 220 (2Θ angle of 12.520 and 42.14). The highest intensity counts in Fig. 7(e) occurred at 365, 250 and 255 (2Θ angle of 15.35, 38.45 and 58.18). These peaks show CNM extract minimally adsorbed onto HCS surface despite its mixed inhibition effect and interfered with the corrosion reaction processes on HCS.

3.5. *ATF-FTIR spectroscopy*

Reactive groups, molecular structures and bonds in CNM oil extract liable for altering the corrosion reaction processes on HCS surface exposed by ATR-FTIR standard Table after ATF-FTIR spectroscopic analysis [59,60]. Fig. 8(a) and (b) depict the spectrum plots for CNM/CH_3COOH and CNM/$C_6H_8O_7$ solution before and after corrosion test for HCS, and from HCS surface after corrosion test within both acids in the presence of CNM extract. Table 3 shows the determined range of wavenumbers following corrosion test for CNM/CH_3COOH solution, CNM/$C_6H_8O_7$ solution, CNM/acid solution on HCS surface, the calculated transmittance, the bonds and reactive groups. Generally, the spectrum plots in Fig. 8(a) depict significant reduction in transmittance at specific range of wavenumbers between CNM/CH_3COOH solution before corrosion, after corrosion test and after corrosion test from HCS surface. The data on transmittance presented in Table 3. The decrease is due to the absorption of the reactive groups within protonated CNM molecules onto HCS surface in CH_3COOH solution. This lead to decrease in their presence within the CNM/CH_3COOH solution. The reactive groups and bonds liable and identified are visible in Table 3. The transmittance data for CNM/CH_3COOH adsorption on HCS surface is even lower but proves the presence of the reactive groups on HCS surface liable for suppression of the redox reactions responsible for corrosion. The spectrum plots in Fig. 8(b) and the corresponding transmittance values in Table 3 shows that at all wavenumber ranges identified, the transmittance for CNM/$C_6H_8O_7$ solution after corrosion test are significantly lower than the transmittance for CNM/$C_6H_8O_7$ solution before corrosion test due to the electrochemical reactions taking place within the degradation and evolution of bonds, and evolution of additional functional groups that were not present before the reaction but subsequently exposed on the spectrum plots. It is also observed that the transmittance

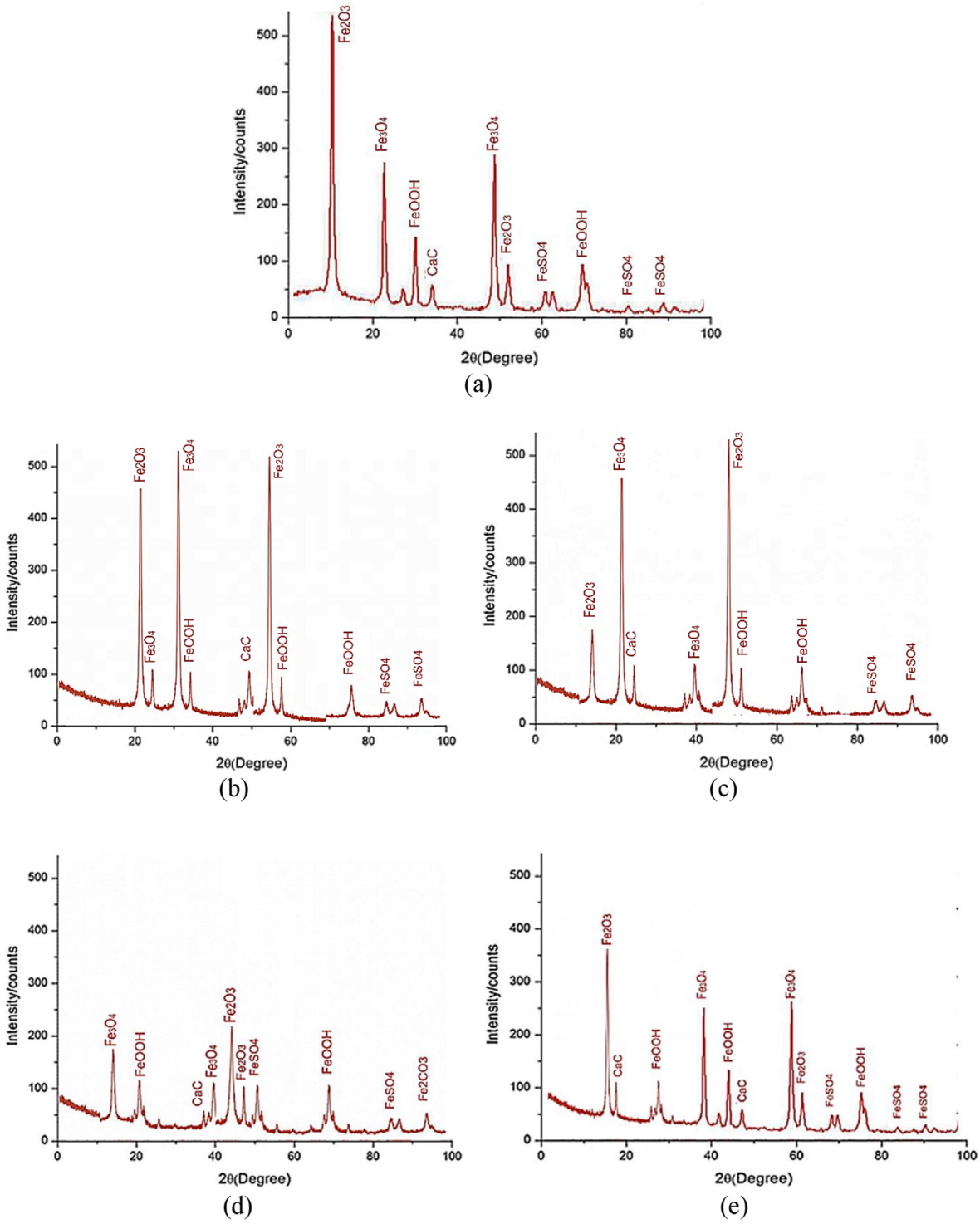

Fig. 7 – XRD Phase identification plots for HCS (a) before corrosion, (b) after corrosion in CH_3COOH solution and (c) after corrosion in $C_6H_8O_7$ solution, (d) after corrosion in CH_3COOH solution at 1.67% CNM concentration and (e) after corrosion in $C_6H_8O_7$ solution at 1.67% CNM concentration.

values generally in $C_6H_8O_7$ solution are generally higher than the values obtained in CH_3COOH solution. This observation indicated that the variation in acidic media influences the performance of corrosion inhibitors and further proves the specific performance nature of the inhibitors. This assertion is proven from the transmittance values for HCS surface after corrosion in CNM/$C_6H_8O_7$ solution. The values show the reactive groups and bonds are present on the surface but have limited influence in suppressing the redox reaction processes responsible for corrosion.

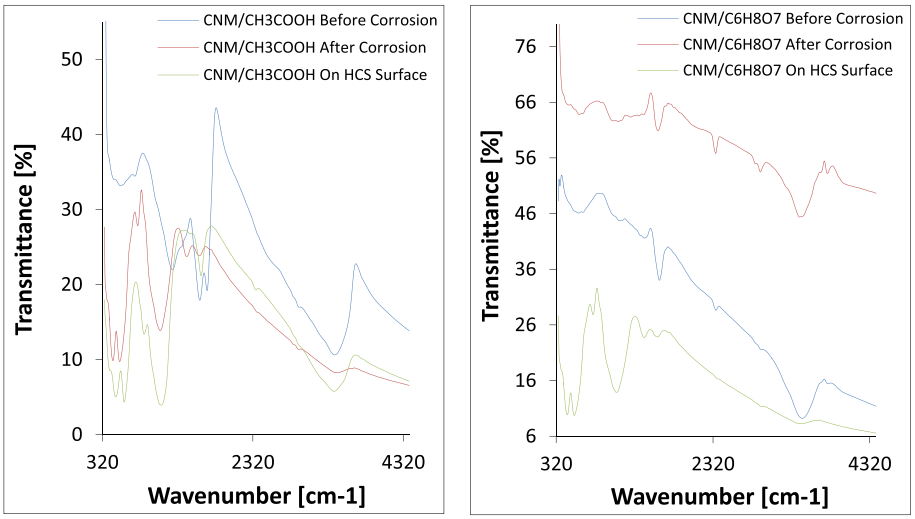

Fig. 8 – ATF-FTIR spectra diagrams of CNM/acid solution before corrosion test, after corrosion test and from HCS surface (a) CNM/CH_3COOH and (b) CNM/$C_6H_8O_7$.

Table 3 – ATR-FTIR spectroscopic data output for CNM/CH_3COOH and CNM/$C_6H_8O_7$ solution, and HCS surface before and after HCS corrosion test.

Wavenumber (cm^{-1})	Transmittance of CNM/CH_3COOH Solution Before Corrosion Test (%)	Transmittance of CNM/CH_3COOH Solution After Corrosion Test (%)	Transmittance of CNM/CH_3COOH Solution On HCS Surface (%)	Bond	Functional Group
CH_3COOH Solution					
550–568	33.18	9.73	8.4	C–Br stretch, C–Cl stretch	alkyl halides
752–872	34.45	27.96	13.4	C–H "oop", N–H wag, =C–H bend	aromatics, primary, secondary amines, carboxylic acid
1096–1260	21.73	13.89	3.94	C–N stretch, C–H wag (–CH_2X), C–O stretch	aliphatic amines, alcohols, esters, ethers
1678–1848	43.15	24.95	27.64	C=O stretch	carbonyls (general), saturated aliphatic, aldehydes, alpha, beta –unsaturated esters, alpha, beta –unsaturated aldehydes, ketones
3422–3444	10.68	8.25	5.85	O–H stretch, H –bonded	Phenols
$C_6H_8O_7$ Solution					
558–620	46.1	63.83	9.85	C–Br stretch, C–Cl stretch	alkyl halides
836–894	49.58	65.97	32.53	C–H "oop", N–H wag, =C–H bend	Alkenes
1094–1096	45.12	62.62	13.89	C–N stretch, C–O stretch	aliphatic amines, carboxylic acids, esters, ethers
1448–1456	41.65	63.03	23.79	C–C stretch (in –ring)	Aromatics
1622–1640	34.06	60.9	23.89	N–H bend	primary amines
2928–2944	21.56	53.51	11.39	C–H stretch	Alkanes
3462–3472	9.26	45.52	8.26	N–H stretch, O–H stretch, H–bonded	primary, secondary amines, amides, alcohols, phenols

4. Conclusion

Admixture of citronella and myrrh essential oil extract significantly suppression the redox electrochemical processes responsible corrosion of high carbon steel in CH_3COOH acid. This was proven from the decrease intensity/counts of active corrosion products in the presence of the oil extract compared to the high intensity counts of the corrosion products without the presence of the extracts. The extract displayed mixed-type inhibition effect with inhibition performance being concentration dependent. Data at rest potentials shows the adsorption processes associated with the extract inhibition increased the thermodynamic instability of the steel surface despite effective inhibition performance. Transmittance values at specific range of wavenumbers shows significant decrease in active functional groups of the extracts after corrosion in CH_3COOH solution which contrast the values obtained from extract/$C_6H_8O_7$ solution. Performance of admixed citronella and myrrh essential oil at all concentrations studied on the carbon steel in $C_6H_8O_7$ acid was significantly below the threshold value for effective corrosion inhibition. The extract interacted with the steel surface, significantly increasing the thermodynamic tendency of the steel to corrode compared to the uninhibited steel in the acid solution.

Declaration of Competing Interest

The authors declare that they have no known competing financial interests or personal relationships that could have appeared to influence the work reported in this paper.

Acknowledgement

The authors appreciate Covenant University for their financial support toward the research in the manuscript.

REFERENCES

[1] Francesco R, Joaquin V. World steel production: a new monthly indicator of global real economic activity. Can J Econ 2020;53(2):743–66.
[2] Loto RT. Comparative study of the pitting corrosion resistance, passivation behavior and metastable pitting activity of NO7718, NO7208 and 439L super alloys in chloride/sulphate media. J. Mats. Res. Techn. 2019;8(1):623–9.
[3] Sastri VS. Challenges in corrosion: costs, causes, consequences, and control. Hoboken: Wiley; 2015. p. 121–3.
[4] James SJ. Oil and gas corrosion prevention. 1st ed. Houston: Gulf Professional Publishing; 2014.
[5] Popoola LT, Grema S, Latinwo GK, Gutti B, Balogun AS. Corrosion problems during oil and gas production and its mitigation. Int. J. Ind. Chem. 2013;4:35. https://doi.org/10.1186/2228-5547-4-35.
[6] Soccol CR, Vandenberghe LPS, Rodrigues C, Pandey A. New perspectives for citric acid production and application. Food Technol Biotechnol 2006;44(2):141–9.
[7] Grewal HS, Kalra KL. Fungal production of citric acid. Biotechnol Adv 1995;13(2):209–34. https://doi.org/10.1016/0734-9750(95),00002-8.
[8] Pandey A, Soccol CR, Rodriguez-Leon JA, Nigam P. Production of organic acids by solid-state fermentation. Solid-state fermentation in biotechnology—fundamentals and applications. New Delhi: Asiatech Publishers Inc.; 2001. p. 113–26.
[9] Vandenberghe LPS, Soccol CR, Pandey AJ, Lebeault JM. Review: microbial production of citric acid. Braz Arch Biol Technol 1999;42:263–76. https://doi.org/10.1007/978-1-4020-9942-7.
[10] Soccol CR, Vandenberghe LPS. Overview of applied solid state fermentation in Brazil. Biochem Eng J 2003;13:205–18. https://doi.org/10.1016/S1369-703X(02)00133-X.
[11] Ivanov ES. Inhibitors of metals corrosion in acid media. Moscow: Metallurgiya; 1986. p. 112–8.
[12] Cheung H, Tanke RS, Torrence GP. Acetic acid. In: Ullmann's encyclopedia of industrial chemistry. Weinheim, Germany: Wiley-VCH GmbH; 2011. https://doi.org/10.1002/14356007.a01_045.
[13] Virginia Department of Health. https://www.vdh.virginia.gov/epidemiology/epidemiology-fact-sheets/acetic%20acid/#:%7E:text=Acetic%20acid%20is%20also%20known,6%25%20acetic%20acid%20in%20water.
[14] Singh MM, Gupta A. Corrosion behavior of mild steel in acetic acid solutions. NACE Corrosion 2000;56. 04.
[15] Kahyarian A, Schumaker A, Brown B, Nesic S. Acidic corrosion of mild steel in the presence of acetic acid: mechanism and prediction. Electrochim Acta 2017;258:639–52. https://doi.org/10.1016/j.electacta.2017.11.109.
[16] Talukdar A, Rajaraman PV. Effect of acetic acid in CO_2-H_2S corrosion of carbon steel at elevated temperature. Mater Today Proc 2022;57(4):1842–5. https://doi.org/10.1016/j.matpr.2022.01.036.
[17] George KS, Nesic S. Investigation of carbon dioxide corrosion of mild steel in the presence of acetic acid— Part 1: basic Mechanisms. NACE Corrosion 2007;63(2):178–86.
[18] Okafor PC, Nesic S. Effect of acetic acid on CO2 corrosion of carbon steel in vapor-water two-phase horizontal flow. Chem Eng Commun 2007;194(2):141–57. https://doi.org/10.1080/00986440600642975.
[19] Singh SK, Mukherjee AK. Kinetics of mild steel corrosion in aqueous acetic acid solutions. J Mater Sci Technol 2010;26(3):264–9.
[20] Rey SP. Carbon steel corrosion control in the past twenty years and in the new millennium. AWT Conference, the National Colloid Company. Carbon steel corrosion control in the past twenty years and in the new millennium. In: AWT conference. The National Colloid Company; 2000.
[21] Matheswaran P, Ramasamy AK. Corrosion inhibition of mild steel in citric acid by aqueous extract of Piper nigrum L. J Chem 2012;9(1):75–8. https://doi.org/10.1155/2012/803098.
[22] Krishnaveni K, Ravichandran J. Effect of aqueous extract of leaves of morinda tinctoria on corrosion inhibition of aluminium surface in HCl medium. Trans Nonferrous Metals Soc China 2014;24(8):2704–12. https://doi.org/10.1016/S1003-6326(14)63401-4.
[23] Ai-Sehaibani H. Evaluation of extracts of henna leaves as environmentally friendly corrosion inhibitors for metals. Mater. Wissen. Werkst. 2000;31(12):1060–3.
[24] Ei-Etre AY, Abdallah M, Ei-Tantawy ZE. Corrosion inhibition of some metals using lawsonia extract. Corrosion Sci 2005;47(2):385–95. https://doi.org/10.1016/j.corsci.2004.06.006.
[25] Raja PB, Sethuraman MG. Inhibitive effect of black pepper extract on the sulphuric acid corrosion of mild steel. Mater

Lett 2008;62(17–18):2977–9. https://doi.org/10.1016/j.matlet.2008.01.087.
[26] Chetouani A, Hammouti B, Benkaddour M. Corrosion inhibition of iron in hydrochloric acid solution by jojoba oil. Pigment Resin Technol 2004;33(1):26–31.
[27] Oguzie EE. Studies on the inhibitive effect of ocimum viridis extract on the acid corrosion of mild steel. Mater Chem Phys 2006;99(2–3):441–6. https://doi.org/10.1016/j.matchemphys.2005.11.018.
[28] Loto RT. Corrosion inhibition effect of non-toxic α-amino acid compound on high carbon steel in low molar concentration of hydrochloric acid. J. Mats. Res. Techn. 2019;8(1):484–93.
[29] Loto CA, Joseph OO, Loto RT, Popoola API. Corrosion inhibitive behaviour of camellia sinensis on aluminium alloy in H_2SO_4. Int J Electrochem Sci 2014;9(3):1221–31.
[30] Isekine I, Hayakawa T, Negishi T, Yuasa M. Analysis for corrosion behavior of mild steels in various hydroxy acid solutions by new methods of surface analyses and electrochemical measurements. J Electrochem Soc 1990;137(10):3029–33. https://doi.org/10.1149/1.2086153.
[31] Singh A, Kalpana S. Inhibition of the corrosion of iron in citric acid solutions by aqueous extract of Fenugreek seeds. Ultra Chem 2012;2:175–9.
[32] Matheswaran P, Ramasamy AK. Corrosion inhibition of mild steel in citric acid by aqueous extract of Piper Nigrum L. E-J Chem. 2012;9(1):75–8.
[33] Anand B, Balasubramanian V. Corrosion behaviour of mild steel in acidic medium in presence of aqueous extract of Allamanda Blanchetii. E-J Chem 2011;8(1):226–30.
[34] Chaudhari HG, Vashi RT. The study of henna leaves extract as green corrosion inhibitor for mild steel in acetic acid. Int. J. Fundam. Appl. 2016;8(2):280–96.